Neutron scattering study of pressure-induced antiferromagnetism in PrSb

D. B. McWhan
Bell Laboratories, Murray Hill, New Jersey 07974

C. Vettier
Institute Laue Langevin, Grenoble 38042, France

R. Youngblood and G. Shirane
Brookhaven National Laboratory, Upton, New York 11973

(Received 21 May 1979)

At low temperatures the $4f^2$ configuration of Pr^{3+} in PrSb approaches a singlet-singlet system at the X point as a result of the crystalline electric field and the anisotropy in the exchange. The energy of the longitudinal exciton decreases with applied pressure, and there is a transition at $T \rightarrow 0$ °K from a Van Vleck paramagnet to an induced-moment antiferromagnet at $P_c = 3.0 \pm 0.2$ GPa. The magnetic structure, phase boundary, and magnetic moment have been determined, and they are in qualitative agreement with a molecular-field model for the transition. Near the critical pressure the longitudinal exciton softens with decreasing temperature and then saturates at a finite energy in the vicinity of the ordering temperature. RPA theories for the dynamics of the singlet-singlet model are not compatible with these results.

I. INTRODUCTION

Praseodymium antimonide is shown to be one of a small class of materials with a singlet ground state in which the evolution of induced-moment magnetism can be studied in detail using the pressure variable. At low temperatures, the crystal-field splitting results in a singlet-triplet system, and the addition of anisotropy in the exchange results in a singlet-singlet system at the X point. There are numerous theoretical studies of such a system of isolated ions which are coupled by exchange.[1,2] Above a critical ratio of exchange to crystal-field splitting, the ground state at $T = 0$ is magnetic with a wave function derived from a mixture of the ground and excited crystal-field states. These models make specific predictions of the moment, the phase diagram, and the temperature dependence of the elementary excitations, and comparisons can be made with PrSb. In addition, the wave-vector dependence of the magnetic excitons yields detailed information on the anisotropy of the exchange interaction, and the pressure dependence of the crystal-field levels can be tested against current theories for crystal fields in metals.

The effect of a crystalline electric field is to partially remove the $(2J + 1)$ degeneracy of the ground-state multiplet ($^3H_4$). Excitations between crystal-field levels have been systematically studied by inelastic neutron scattering techniques in a number of rare-earth intermetallic compounds.[3] The observed energy levels and cross sections for scattering are in good agreement with a model based on isolated single ions. In the cubic NaCl structure, the crystal-field Hamiltonian is of the form

$$H = W\left[\frac{x}{F(4)}\left(O_4^0 + 5O_4^4\right) + \frac{1-|x|}{F(6)}\left(O_6^0 - 21O_6^4\right)\right] ,$$

where O_n^m is an operator equivalent and F(n) is a tabulated numerical factor.[4] The two adjustable parameters are W, a scale factor, and x, the ratio of the fourth to sixth degree terms. For PrSb neutron scattering studies on polycrystalline samples give values of $W = 4.4$ °K and $x = -0.966$.[3] In a simple point-charge model these parameters vary as

$$Wx \propto (Ze^2/R^5)\langle r^4\rangle ,$$

$$W(1-|x|) \propto (Ze^2/R^7)\langle r^6\rangle ,$$

where Z is the effective charge on the ligands which are at a distance, R, from the rare-earth ion and $\langle r^n\rangle$ is the appropriate average of the $4f$ radial wave function. R has been changed chemically by varying the rare-earth ion, which results in the well-known lanthanide contraction. For reasonable choices of Z and $\langle r^4\rangle$, the R^5 dependence, predicted by the point-charge model, was observed across the light rare-earth pnictides and chalcogenides.[5] This simple picture has been questioned as a result of measurements of the Knight shift[6] and magnetic susceptibility[7] as a function of pressure. More recently, direct measurements of the effect of pressure on several crystal field levels of PrSb were made using neutron scattering techniques, and they confirm that the point-charge model gives not only the wrong magnitude but the wrong sign for the pressure dependence.[8]

These measurements have been extended to higher pressures, and the results are presented in Sec. IV B.

Most of the previous neutron scattering studies of crystal-field excitations in rare-earth intermetallic compounds have been made using polycrystalline samples, and it has been assumed that the exchange is isotropic. This would lead to some dispersion in the magnetic excitons, but not to a lifting of the degeneracy of the triplet. More recent neutron scattering studies, using single crystals of PrSb, revealed that the degeneracy is lifted along [001] which indicates that the exchange is anisotropic.[8] These results are summarized in Sec. IV A. The important part of this work from the experimental point of view is that there is a substantial softening of the longitudinal magnetic exciton at the X point [(0,0,1) or (1,1,0) in the NaCl structure] and that the system approaches a singlet-singlet model at low temperatures. In addition, the energy of the exciton decreases with increasing pressure as a result of the overall decrease in the crystal-field splitting. This results in an increase in the ratio of exchange to crystal-field splitting toward the critical ratio for the onset of induced-moment magnetism; preliminary evidence for this transition has been presented.[8] The phase boundary for this transition in the pressure-temperature plane is presented in Sec. III B and the determination of the magnetic structure in Sec. III C.

The detailed behavior at the transition to the induced-moment magnetic state has received considerable theoretical and experimental attention.[1,2] In the simplest molecular-field model for a singlet-singlet system, the magnetic susceptibility varies as

$$\frac{1}{\chi(\vec{q})} = \frac{\Delta}{2g^2\beta^2\alpha^2}\left[\frac{1+e^{-\Delta/kT}}{1-e^{-\Delta/kT}} - \frac{4J(\vec{q})\alpha^2}{\Delta}\right],$$

where Δ is the separation, α is the J_z matrix element between the two singlet levels, and

$$J(\vec{q}) = \sum_j J_{ij}\exp[i\vec{q}\cdot(\vec{r}_i - \vec{r}_j)] \ .$$

If $4J(\vec{q})\alpha^2/\Delta$ exceeds 1, the susceptibility $\chi(\vec{q})$ diverges at some finite temperature, leading to a magnetic ground state. This ratio has been varied chemically in the systems $Tb_xY_{1-x}Sb$ (Ref. 9) and $Pr_{3-x}La_xTl$ (Ref. 10), and the variation of ordering temperature T_c and magnetic moment σ are in qualitative agreement with molecular-field calculations using the full crystal-field level schemes. Direct measurements of T_c and σ as a function of pressure through the critical region in Pr_3Tl are also only in qualitative agreement with either the molecular-field model or the collective-excitation model.[11] Our results on PrSb above the critical pressure are similar to these earlier studies in that only qualitative agreement with these models is found, as discussed in Sec. V.

The behavior of the collective excitations in induced-moment systems is still under active study. If the transition is second order, then there must be a critical slowing down of the appropriate dynamic fluctuation at the ordering temperature, and in the case of a singlet-singlet system, it is the longitudinal magnetic exciton which goes soft. Early attempts[12] to verify this soft-mode behavior in polycrystalline samples of Pr_3Tl by neutron scattering failed because the appropriate soft mode in a singlet-triplet system (within RPA) results from excitations within the degenerate triplet state.[13–16] The predicted appearance of critical scattering resulting from these excitations, which diverges at the transition, has been observed in Pr_3Tl.[17] The measurements on PrSb of the temperature renormalization of the exciton above P_c are reported in Sec. IV C, and the results are shown to be incompatible with theoretical models for the singlet-singlet system in Sec. V.

The outline of this paper is as follows: Sec. II gives a description of the sample preparation and the apparatus used to do neutron scattering measurements at high pressure and low temperature. The elastic scattering measurements are presented in Sec. III and are subdivided into the determinations of the equation of state; the magnetic phase diagram; and the magnetic structure. The inelastic scattering measurements are given in Sec. IV and are subdivided into crystal-field levels at 1 atm.; the pressure dependence of the crystal-field levels; and the temperature dependence of the collective excitations above the critical pressure. Finally the results are discussed in relation to current theoretical models in Sec. V.

II. EXPERIMENTAL

Crystals of PrSb were grown by L. D. Longinotti. The elements were prereacted in an evacuated quartz tube, and then the PrSb was resealed in a tantalum tube. The latter was heated resistively in vacuum to above the melting point of PrSb and then cooled slowly. The neutron scattering measurements at 1 atm were made on a cylindrical sample ~4 mm in diameter and ~2 cm long. The crystals tend to cleave perpendicular to the fourfold axis, and the samples used in the experiments at high pressure were cleaved or cut from a second crystal so as to give an $(hk0)$ scattering plane in the high-pressure cell. These samples were typically $3.5\times3.5\times8$ mm^3 (~0.09 cm^3). The magnetic phase diagram was determined using a powder sample obtained by crushing the small pieces of the second crystal that remained after preparing the samples for the inelastic studies.

The neutron scattering measurements were done at both Brookhaven National Laboratory and the Institute Laue Langevin. The compressibility and magnetic phase boundary were determined on the double-axis spectrometers D1A and D2 at the I.L.L.

One set of inelastic measurements at 2.3 GPa was done on IN8, and the bulk of the inelastic measurements was done on triple-axis spectrometers at the Brookhaven high-flux beam reactor. Pyrolytic graphite crystals were used as monochromator, analyzer, and filter. Most of the data were obtained using constant-Q energy scans with fixed incident or analyzer energy of 14.8 or 13.5 meV and various combinations of 20- and 40-min collimation.

In the earlier study of the pressure dependence of the crystal-field levels in PrSb a special combination cryostat and hydraulic press was used to apply the pressure to the sample *in situ* and to cool the pressure cell using a closed cycle helium refrigerator.[8] The sample could not be cooled below $T \approx 25\,^{\circ}K$ in this apparatus, and it was necessary to use clamp devices in the present work. The clamp device used at I.L.L. is presented in Ref. 18, and the clamp device used at Brookhaven is shown in Fig. 1. The pressure vessel is a barrel-shaped cylinder of high-density polycrystalline Al_2O_3. The mating steel (Vascomax 300) support pieces have left- and right-handed threads and are screwed into the aluminum alloy (7075-T6) locking sleeve. The interface between the support pieces and the Al_2O_3 is coated with MoS_2 (Molycote) to reduce friction. (The use of Pb foil instead of MoS_2 did not result in enough end support relative to radial support and was less satisfactory in reaching pressures above 3 GPa.) The steel support pieces were pressed together in a hydraulic press with an applied load of 30 tons. The locking sleeve was tightened, and the applied load removed, transferring the load to the locking sleeve. The retained load was monitored by a bridge of four strain gauges (WK-09-031CF-350 type gauges manufactured by Micro-Measurements, Romulus, Michigan) attached to the thinner portion of the sleeve.

The crystal was mounted inside the Al_2O_3 cylinder in an aluminum cell (5052) using beryllium copper extrusion rings and cap to contain a liquid pressure transmitting medium. A number of different cell geometries were tried, but as yet it has not been possible to contain a 4:1 deuterated methanol-ethanol mixture above 3-3.5 GPa without cell failure. Longitudinal cracks develop in the Al_2O_3 cylinder in the unsupported area which forms the window between the steel pieces. As the inside of the Al_2O_3 cylinder expands the Al cell fails and the fluid escapes. In addition, the restricted size of the cell has to be balanced against the minimum size of the crystal which can be used in the neutron scattering experiment. As a result, the walls of the Al cell are thinner than the optimum dimensions for retaining an unsupported area seal to the cap.[19] As a compromise the total compression of the cell was minimized by filling most of the space between the crystal and the cell walls with carefully machined pieces of pure lead. The pressure fluid used to fill the rest of the space was

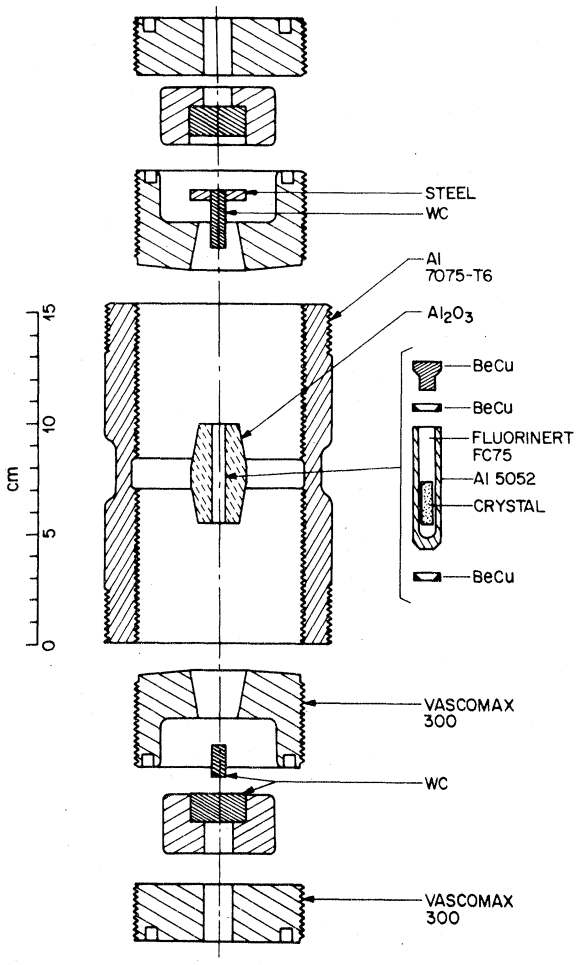

FIG. 1. Exploded view of clamp device for neutron scattering at pressures up to 4.5 GPa and low temperatures. The external support for the Al_2O_3 and the pressure applied by tungsten carbide pistons are both clamped by an aluminum locking sleeve with left- and right-handed threads on the bottom and top halves, respectively.

Fluorinert FC-75. This material becomes glassy above ~2 GPa. This is evident in the mosaic spread of the PrSb which remained unchanged at a full width at half maximum (FWHM) of 0.2° up to 2 GPa and then increased smoothly to 1.7° at 3.4 GPa.

In order to apply the pressure to the sample, one mounts the clamp device in a small hydraulic press on the spectrometer. The cell is held by a collar at the top, and the load transmitted to the sample via the series of tungsten carbide pistons and back-up blocks. In this way the locking sleeve is stretched, thus minimizing the loss of load when releasing the applied force. The lattice parameter of the sample and that of the lead is monitored until the desired parameter has been achieved. The load is locked, and the clamp device is transferred to a Cryogenics

Associates CT-14 temperature-control cryostat. An extra temperature sensor is mounted on the bottom of the cell to check for possible temperature gradients across the clamp device.

There is friction in the apparatus so that the true pressure on the sample is only ~80% of the applied load. Because it would require a decrease of several tenths of a GPa to reverse the friction, almost no pressure is lost on the sample during the locking operation. In addition, the larger thermal contraction of the Al sleeve relative to the steel and tungsten carbide pieces partially offsets the thermal contraction of the pressure transmitting medium so that the change in pressure on cooling is probably less than 0.1 GPa.

III. ELASTIC SCATTERING

A. Equation of state

The important variable is interatomic spacing or volume, but it is of interest to be able to convert a volume change into a corresponding pressure. The equation of state for PrSb has been measured at room temperature and extrapolated to $T=5\,^{\circ}\mathrm{K}$ using the Mie-Grüneisen equation of state. The results are consistent with both ultrasonic measurements of the bulk modulus in the limit $P\rightarrow 0$, B_0, and measurements of the phonon dispersion relations.

Neutron scattering measurements were made at I.L.L. on a double-axis spectrometer, D1A, using a single crystal of PrSb embedded in polycrystalline NaCl. The pressure was obtained from the lattice parameter of NaCl using the Decker equation of state,[20] and the results are shown as filled circles in Fig. 2. Two points (closed triangles) were obtained during the course of the inelastic measurements at BNL; the value of the pressure was obtained from the lattice parameter of lead using the Birch equation,

$$P=\tfrac{3}{2}B_0(y^7-y^5)[1-(3-\tfrac{3}{4}B_0')(y^2-1)] ,$$

where

$$B_0=-\left(\frac{dP}{d\ln V}\right)_{P\rightarrow 0} ,$$

$$B_0'=\left(\frac{dB_0}{dP}\right)_{P\rightarrow 0} ,$$

$$y=a_0/a .$$

The values of the constants used for Pb are B_0 = 41.89 GPa, B'_0 = 5.72, and $a_0=4.9504$ Å.[21] The estimated error is ± 0.1 GPa in the pressure and ± 0.1% in the lattice parameter. Because the measurements extend over a limited range of pressure and are of limited accuracy, it is not possible to determine

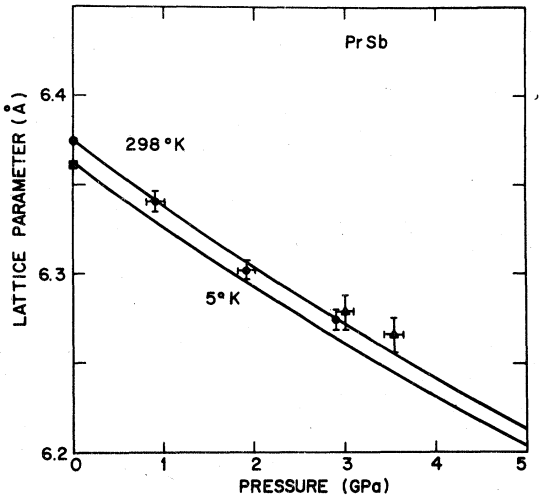

FIG. 2. Equation of state of PrSb at $T=298$ and 5 °K. Upper curve is a Birch equation with $B_0=56$ GPa. Lower curve obtained assuming a thermal pressure of 0.38 GPa.

both B_0 and B'_0 for PrSb, so the data in Fig. 2 were fit to the Birch equation assuming $B'_0=4$, i.e., that the last term in the Birch equation is zero. This gives $B_0=56$ GPa; the resulting calculated equation of state is the upper solid line in Fig. 2. This is consistent with the ultrasonic value of 51 GPa,[22] and the values for LaSb (Ref. 23) and NdSb (Ref. 24) of 56 and 47 GPa, respectively, obtained from the phonon dispersion relations. The lower value of B_0 obtained from the ultrasonic measurements, and the fact that the points at the highest pressure lie above the calculated curve in Fig. 2, suggests that $B'_0>4$. Without more accurate measurements a more detailed fit is not warranted.

To obtain an equation of state at $T=5\,^{\circ}\mathrm{K}$ it is assumed that the equation can be separated into a volume term at $T=0$ and a thermal pressure which is dependent on temperature but not on volume. The lower curve in Fig. 2 has been constructed by subtracting a constant pressure of 0.38 GPa from the curve for room temperature so that the curve passes through the value for the lattice parameter at $T=5\,^{\circ}\mathrm{K}$ and $P=1$ atm. The pressures reported below were obtained from the measured lattice parameter at low temperatures and the lower curve in Fig. 2.

B. Magnetic phase diagram

The phase boundary was determined by measuring the intensity of the (110) magnetic reflection as a function of temperature at different values of the lattice parameter. Measurements were made on a polycrystalline sample of PrSb on D2 at I.L.L. down to $T=2\,^{\circ}\mathrm{K}$ and on a single crystal at BNL. Typical data

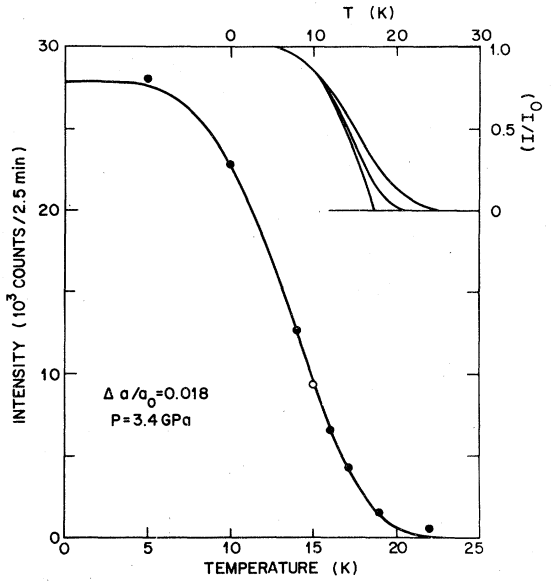

FIG. 3. Intensity of (110) magnetic reflection versus temperature at $P=3.4$ GPa. Closed circles taken on warming and open circle on cooling. Inset shows model calculations of the intensity assuming a Gaussian distribution of pressure in the sample with a width of 0, ±5%, and ±10%. The curve through the data is the calculated curve corresponding to the ±5% spread in pressure.

from the latter experiment is shown in Fig. 3 for a lattice-parameter decrease of $(a_0-a)/a_0=0.0178$. Extrapolating the magnetic intensity to zero gives a transition temperature of $T_N=18\pm1$ °K. The results of both experiments are summarized in Fig. 4. The critical lattice-parameter change and pressure for the onset of antiferromagnetism in the limit of $T=0$ °K

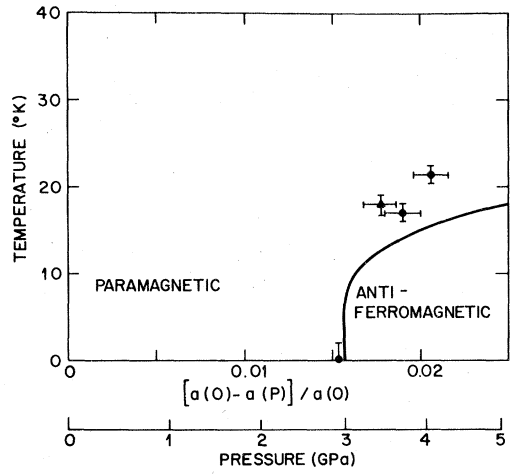

FIG. 4. Phase diagram for PrSb. Solid curve is calculated for the singlet-singlet model in the molecular-field approximation as described in the text. The pressure scale is taken from Fig. 3 using the lattice parameter change at $T=5$ °K.

are $(a_0-a)/a_0=0.016\pm0.001$ and $P=3.0\pm0.2$ GPa, respectively.

The data in Fig. 3 show a continuous change in intensity through the ordering temperature, and the open circle which was measured on cooling instead of warming gives no indication of hysteresis in the transition. As discussed below, the magnetic structure is antiferromagnetic of type I with the moments parallel to the propagation vector; in that case, the renormalization-group theory predicts a continuous transition. However, the curve is quite rounded above T_N. This might result from a nonuniform pressure distribution across the sample or from critical scattering. An estimate of the pressure gradient necessary to produce the observed broadening can be made as follows. Assume a molecular-field model with spin $\frac{1}{2}$ for the order parameter, a moment at $T=0$ °K which varies linearly with T_N, a phase boundary of the form $T_N(\Delta a/a_0)=A(\Delta a/a_0-B)^{1/2}$, and a Gaussian distribution of lattice parameters, $\Delta a/a_0$, with a standard deviation of σ. The inset in Fig. 3 shows the resulting curves of intensity versus temperature for $\sigma=0$, 0.0008, and 0.0016. These correspond to pressure distributions of 0, ±5%, and ±10%, respectively. The curve through the data points in Fig. 3 is the calculated curve for $\Delta P/P=\pm0.05$, and the good agreement suggests that this is a reasonable estimate for the pressure distribution.

Clearly defined quasielastic critical scattering was not observed. There is elastic scattering above T_N, but a large part of this may result from the pressure distribution. Longitudinal scans through (110) with $\Delta E=0$ show that this elastic scattering is resolution limited even at $T=25$ °K. If this is critical scattering, then at $T/T_N=1.39$ the correlation length still exceeds 150 Å.

C. Magnetic structure

As discussed below, the inelastic scattering measurements show that the longitudinal magnetic exciton goes soft at the X point (001 or 110 points in the Brillouin zone of the NaCl structure). This suggests that the magnetic structure will propagate with a set of $\vec{q}$ vectors belonging to the star of ⟨100⟩ and that the Fourier components of the magnetic moment are parallel to the ⟨100⟩ directions. A Landau expansion of the free energy for the NaCl structure shows that there are only two fourth-order invariants. The free energy can be minimized with either a single- or a triple-$\vec{q}$ state. If the structure propagates with a single $\vec{q}$, then the symmetry will be tetragonal with magnetic domains. This structure will be a type-I antiferromagnet with the moment along the c axis and alternating ferromagnetic sheets stacked antiferromagnetically along c. If the structure propagates with a triple $\vec{q}$ state, then the symmetry will be cubic

with no lattice distortion. The magnetic structure will be noncollinear. As the observed magnetic scattering does not have cubic symmetry, we interpret our results using a type-I structure with an uneven distribution of domains resulting from a uniaxial component to the applied pressure.

The intensity of the magnetic scattering for this structure is given by

$$I_{\text{mag}}(hkl) = c\left[1 - \frac{l^2}{h^2+k^2+l^2}\right]|F(hkl)|^2 ,$$

$$F(hkl) = 0.2693\mu f(hkl) \times (1 + e^{i\pi(h+k)} - e^{i\pi(h+l)} - e^{i\pi(k+l)}) ,$$

where μ is the magnetic moment in Bohr magnetons and $f(hkl)$ is the magnetic form factor which is taken from Ref. 25. The first term on the right within parentheses reflects the fact that the intensity varies as the square of the projection of the moment perpendicular to the scattering vector, $\vec{Q}$. For example, the intensity of the (001) is zero because $\vec{Q} \| \vec{\mu}$ whereas the (100) and (010) are zero because of the structure factor $F(hkl)$.

In the present experiments at high pressure, there is a small uniaxial component on the sample because the apparatus employs a piston-cylinder geometry and because the pressure medium has become glassy. Since the sample is mounted with a cubic axis parallel to the direction of the uniaxial stress, there will be a strong preference for domains with the magnetic axis perpendicular to the scattering plane. Examination of the equation above reveals that there is no overlap of magnetic scattering from different domains in a single crystal so that the domain distribution can be uniquely determined.

The integrated intensity of all $(hk0)$ reflections was measured using θ-2θ scans with $k_i = 2.590$ Å^{-1} and 20-40-40-40 collimation both above and below the ordering temperature of $T_N = 18$ °K at $P \approx 3.4$ GPa. The magnetic intensity, taken as the difference between the measured intensity at the two temperatures, was put on an absolute scale by comparison with the nuclear intensity. The scattering lengths are $b_{\text{Pr}} = 0.44\times10^{-12}$ cm and $b_{\text{Sb}} = 0.56\times10^{-12}$ cm so that for the allowed reflections $I_{\text{nuc}}(hkl) = 16c(0.44 \pm 0.56)^2$ with (+) for hkl all even and (−) for hkl all odd.[26] There is a nonuniform distribution of crystallites, so the average of the neighboring nuclear peaks was used to put each magnetic intensity on an absolute scale. The magnetic intensities calculated for a magnetic moment of 1.45 μ_B and a domain distribution of 0.02, 0.10, 0.88 for [100], [010], [001] domains, respectively, are compared with the observed intensities in Table I. There is reasonable agreement indicating that the structural assignment is correct.

TABLE I. Comparison of calculated and measured magnetic intensities for PrSb in type-I antiferromagnetic structure.

h,k	Domain	I_{calc}	I_{obs}
1,0	all	0	<0.01
1,1	[001]	1.98	1.99
1,2	[100]	0.03	0.03
2,1	[010]	0.16	0.20
3,0	all	0	<0.005
1,3	[001]	1.46	1.51
3,1	[001]	1.46	1.55
2,3	[010]	0.04	0.05
3,2	[100]	0.01	0.02
1,4	[100]	0.02	0.04
4,1	[010]	0.12	0.08
3,3	[001]	1.07	1.00
$\mu = 1.45\mu_B$		$\Delta a/a_0 = -0.018$	

Domain	Fraction	$T_N = 18$ °K
[100]	0.02	
[010]	0.10	
[001]	0.88	

An independent determination of the magnetic moment was obtained from experiments on a polycrystalline sample at $P \approx 3.4$ and 4.0 GPa with corresponding $T_N = 17$ and 21.5 °K. The ratios of the intensities of the (110) and (200) reflections lead to moments of $(1.1 \pm 0.2)\mu_B$ and $(1.2 \pm 0.2)\mu_B$. These values are smaller than that obtained in the single-crystal work above, and we take as a reasonable value for the moment $(1.3 \pm 0.2)\mu_B$ for an ordering temperature of $T_N \approx 18$ °K.

IV. INLASTIC SCATTERING

A. Crystal-field levels

The average crystal-field levels for PrSb have been determined using polycrystalline samples and time-of-flight techniques.[3] The energies and intensities of the observed spectra were fit quite well using a single-ion model for the Pr^{3+} ($J = 4$) in the NaCl structure which leads to four allowed magnetic dipole transitions, Γ_1-Γ_4, Γ_4-Γ_3, Γ_4-Γ_5, and Γ_3-Γ_5. Symmetry considerations show that the degeneracy of Γ_4, Γ_3, and Γ_4 states may be lifted when going away from the Γ point ($q=0$) to a nonzero $\vec{q}$ point in the Brillouin zone. This is shown schematically in Fig. 5, where the lifting of degeneracies is shown in the three major symmetry directions. For example, if the single ions are coupled by anisotropic exchange, then

many of the remaining degeneracies are lifted.

Within the dipole approximation, the partial differential cross section per ion for the transition $\Gamma_i \rightarrow \Gamma_j$ is

$$\frac{d^2\sigma}{d\Omega\, d\omega'} = \left(\frac{\gamma e^2 g F(\vec{Q})}{2m_e c^2}\right)^2 \frac{k'}{k} \sum_{\alpha\beta} (\delta_{\alpha,\beta} - \hat{q}_\alpha \hat{q}_\beta) \sum_{\nu_i,\nu_j} P_i \langle \Gamma_i \nu_i | \vec{J}_\alpha^* | \Gamma_j \nu_j \rangle \langle \Gamma_j \nu_j | \vec{J}_\beta | \Gamma_i \nu_i \rangle \delta(\hbar\omega + \hbar\omega_i - \hbar\omega_j) \ ,$$

where P_i is the population and ν_i the individual eigenvectors of the Γ_i (or Δ_i, Σ_i, and Λ_i) representation and α and β refer to the components of $\vec{J}$[27]; $\hat{q}$ is the unit vector parallel to the scattering vector $\vec{Q} = \vec{\tau} + \vec{q}$ where $\vec{\tau}$ is a reciprocal-lattice vector. Symmetry-adapted wave functions at $\vec{q}$ can be determined, in the absence of interion coupling, by projecting the Γ-point wave functions into the representations of the little group $\vec{G}_q$. Longitudinal modes are associated with J_z, while transverse modes are induced by $J_\pm$ operators. In Fig. 5, allowed magnetic dipole transitions are indicated as solid vertical lines for the longitudinal magnetic excitons and dashed lines for the transverse excitations. They can be distinguished by their dependence on $\vec{Q}$. The energies at Γ correspond to those obtained from time-of-flight measurements. No attempt has been made to determine the $\vec{q}$ dependence of all the crystal-field levels, and we have restricted our study to excitations out of the singlet ground state which can be observed at low temperatures. It can be seen from Fig. 5 that most of the transitions between the Γ_1 and Γ_4 levels are allowed, and they can be distinguished by observing the dependence on $(\delta_{\alpha,\beta} - \hat{q}_\alpha \hat{q}_\beta)$. For example, (0,0,1) and (1,1,0) are equivalent X points in the Brillouin zone, but as shown in Fig. 6, the X_4 exciton is only observed at 110 where the J-operator component associated with Σ_4 is perpendicular to $\vec{Q}$ as indicated in the inset. Measurements along $[11\zeta]$, $[22\zeta]$, $[\zeta\zeta\zeta]$, and $[1+\zeta\ 1-\zeta\ 1-\zeta]$ indicate that although allowed by symmetry, there is no measurable lifting of the degeneracy between the Σ_2 and Σ_3 levels or between the Λ_2 and Λ_3 levels. The resulting measured dispersion relations and level assignments for the transitions between the ground state and the lowest excited states are shown in Fig. 7.[8] There is a pronounced softening of the longitudinal magnetic exciton, Δ_1', near the X point, and the large slope of the dispersion relation near X indicates that the interaction causing the softening is long range.

A final point about the crystal-field levels at 1 atm is the complexity at higher temperatures as revealed in the single-crystal results. With increasing tempera-

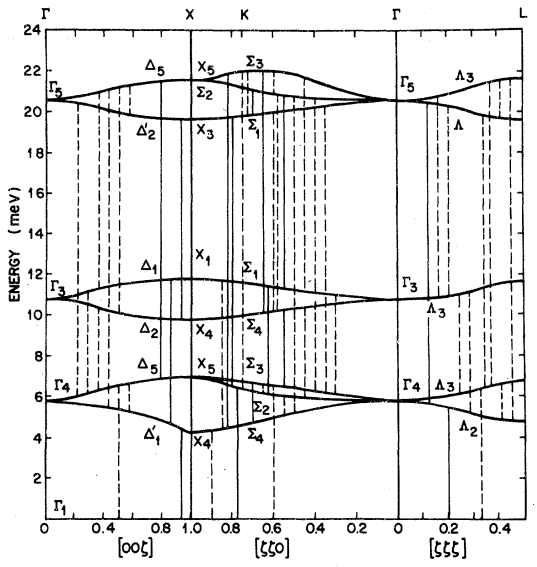

FIG. 5. Schematic lifting of the degeneracy of the Γ_4, Γ_3, and Γ_5 crystal-field levels along the Δ, Σ, and Ω directions which are allowed by group theory. Crystal-field transitions allowed in the dipole approximation are indicated by solid vertical lines and dotted lines for longitudinal and transverse magnetic excitons, respectively.

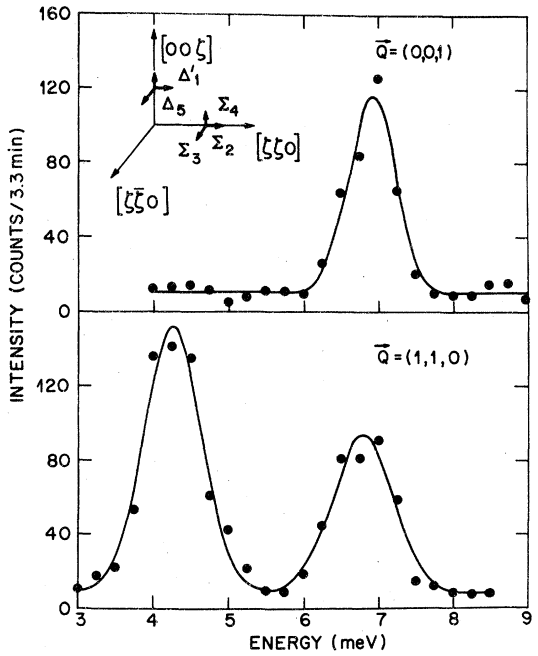

FIG. 6. Typical data obtained in the (hhl) scattering plane at $\vec{Q}$ = (0,0,1) (top) and (1,1,0) (bottom) showing the dependence on the projection of $\vec{J} \perp \vec{Q}$. The inset shows that the longitudinal magnetic exciton can be observed along the Σ line, Σ_4, but not along Δ, Δ_1'.

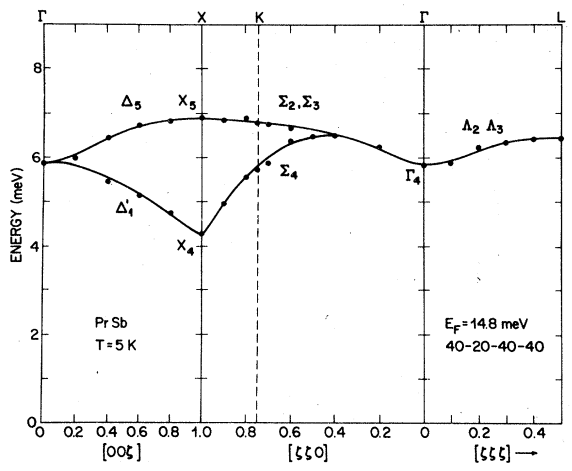

FIG. 7. Lifting of the triple degeneracy of the Γ_1-Γ_4 magnetic exciton. Note splitting is only along [001] and not along [111] although both are allowed (Fig. 5). The lines are guides to the eye.

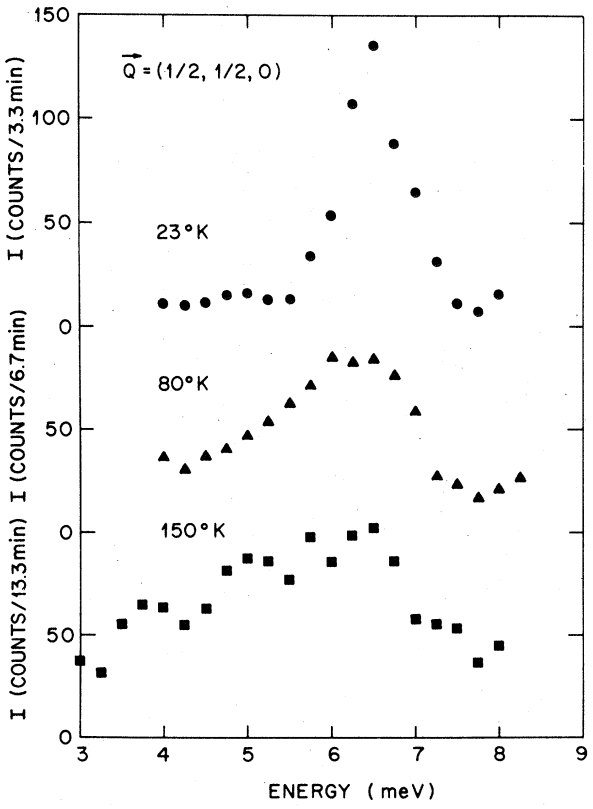

FIG. 8. Decrease in the intensity of the magnetic excitons at $\vec{Q}=(\frac{1}{2},\frac{1}{2},0)$ with increasing temperature. Note excitons coming from Γ_1-Γ_4 levels decrease as expected while those from Γ_4-Γ_3 increase much less than expected from the single-ion model.

tures in a single-ion model, the intensity of the Γ_1-Γ_4 excitons between 6 and 7 meV will decrease as the population of the ground state decreases. The intensity of the Γ_4-Γ_3 excitions at 4–5 meV grows to be the dominate feature in the observed spectra from polycrystalline samples which average over all q space. In Fig. 8 measurements on a single crystal at $\vec{Q}=(\frac{1}{2},\frac{1}{2},0)$ at three temperatures are compared. In contrast with the results on polycrystalline samples, the Γ_1-Γ_4 exciton decreases roughly as expected, but the Γ_4-Γ_3 exciton is observed with an intensity which is a factor of 10 lower than that expected on the basis of the simple population and matrix element arguments. Although the broad features observed in the polycrystalline results are compatible with single-ion modes, the detailed behavior is clearly more complex.

B. Pressure dependence of crystal-field levels

The success of the point-charge model in fitting the observed crystal-field spectra for a number of rare-earth intermetallic compounds of varying lattice parameters has not been carried over to measurements as a function of pressure. In a point-charge model the parameters W and x vary as[28]

$$\frac{dW}{da}=-(7-2|x|)\ ,$$

$$\frac{dx}{da}=2(1-|x|)\ .$$

For PrSb with $x=0.966$ the logarithmic derivatives are -5.1 and 0.07, respectively. Indirect determinations of the Γ_1-Γ_4 exciton as a function of pressure have been made from NMR (Ref. 6) and magnetic susceptibility measurements.[7] Assuming no change in x, these results suggest that the point-charge model for the variation of W with pressure is wrong not only in magnitude but also in sign. Using neutron scattering both the Γ_1-Γ_4 and Γ_4-Γ_5 transitions have been studied directly as a function of pressure.[8] Within experimental error, there is no change in x, and it is the scale factor W which decreases with increasing pressure. At the present time no satisfactory theory has been given to explain these results. Clearly crystal fields in metals are more subtle than a point-charge model.

The measurements of the excitions at Γ and X have been extended to 3.4 GPa, and the results are shown in Fig. 9. The points at $\Delta a/a_0=0$ and 0.001 are from our earlier work. The points at $\Delta a/a_0=0.015$ were obtained at I.L.L. and those at 0.018 at Brookhaven. The former were at $T=2$ °K and the latter at 40 °K. As described in Sec. IV C, there is a temperature renormalization of the excitons at $\Delta a/a_0=0.018$, and the data at $T=40$ °K approxi-

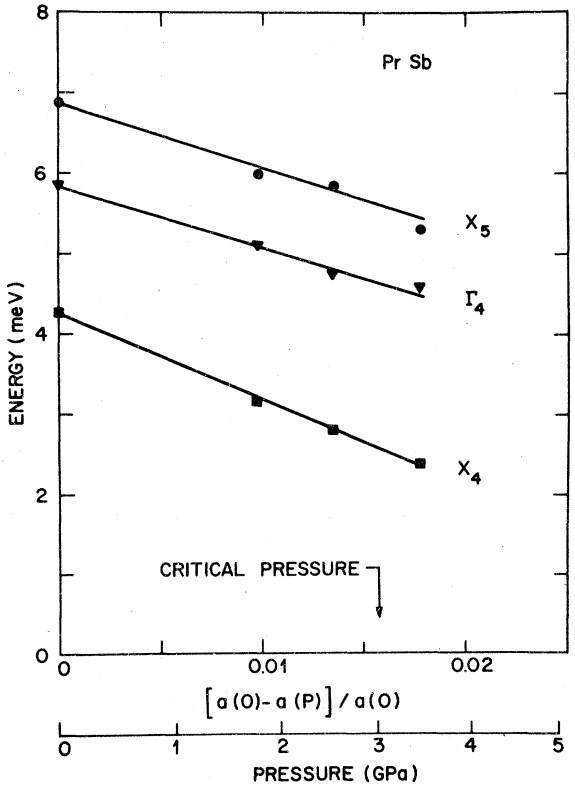

FIG. 9. Variation with pressure (volume) of the energy of the excitons at Γ and X. As the three energies have similar pressure dependences, one concludes that $J(\vec{q})$ is constant and the major effect of pressure is on Δ. Lines are guides to the eye.

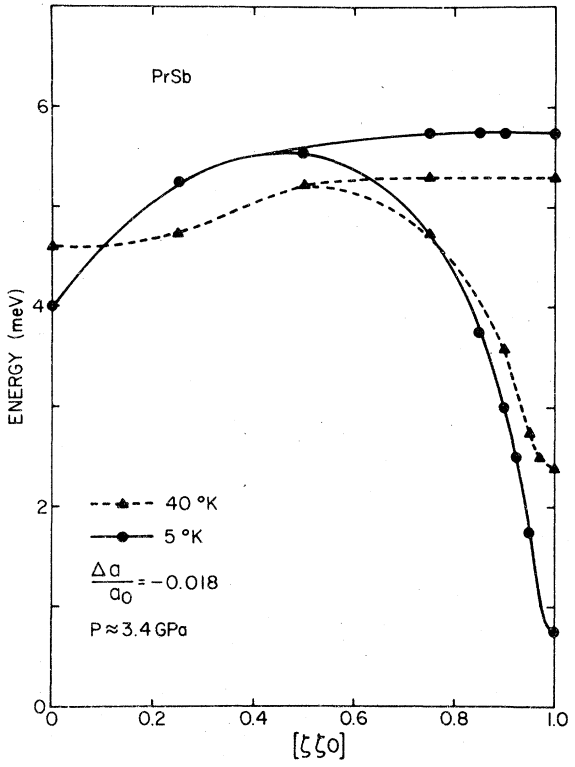

FIG. 10. Renormalization with temperature of the excitons along $[\zeta\zeta 0]$ at $P=3.4$ GPa which is above the critical pressure for antiferromagnetism. Lines are guides to the eye.

mate the high-temperature value. Within experimental error, there is a linear decrease in the exciton energy with decreasing interatomic spacing, with a slope of $dE/da = 12.2 \pm 1.5$ meV/Å. In the limit of 1 atm., the logarithmic derivative at the zone center is $d\ln E/d\ln a = 13 \pm 2$. This number is in good agreement with recent low-temperature thermal expansion measurements which give a value of 12.[29]

C. Temperature dependence of the collective excitations above the critical pressure

In Secs. I–IV the static properties of the induced-moment antiferromagnetism and the existence of a soft magnetic exciton as a function of pressure in PrSb have been established. In this section the spin dynamics above the critical pressure are presented, and the evolution of the crystal-field levels with increasing temperature is studied. All of these measurements were made at Brookhaven on a crystal mounted to give an $(hk0)$ scattering plane in a clamp device at a pressure of 3.4 GPa ($\Delta a/a_0 = 0.018$). As shown in Fig. 4, the Néel temperature is 18 °K at this pressure. Measurements were made as a function of temperature between 5 and 40 °K and as a function of $\vec{q}$ in the $[\zeta\zeta 0]$ direction.

The dispersion relations along $[\zeta\zeta 0]$ at 5 and 40 °K are shown in Fig. 10. In contrast to data taken at 1 atm. and 1.6 GPa, there is a marked temperature dependence. The dispersion relations near the magnetic zone center, (1,1,0), are shown in more detail in Fig. 11 where abscissa is $(1-\zeta, 1-\zeta, 0)$ and representative data are shown in Fig. 12. There is a marked softening at the magnetic zone center and a small change in the apparent shape of the curves near the ordering temperature. The saturation of the energy as a function of decreasing temperature is shown in Fig. 13 along with the temperature dependence at several other values of $\vec{Q}$.

There can be a large experimental uncertainty in the energy of the magnetic excitations at small q. This comes about because of the finite size of the spectrometer resolution function. While this effect is responsible for a larger error bar on the excitation at $\vec{Q} = (1, 1, 0)$, we can still rule out complete softening of this mode. First, numerical calculations for the actual experimental conditions show that the shift of the apparent peak position is large only for gaps less

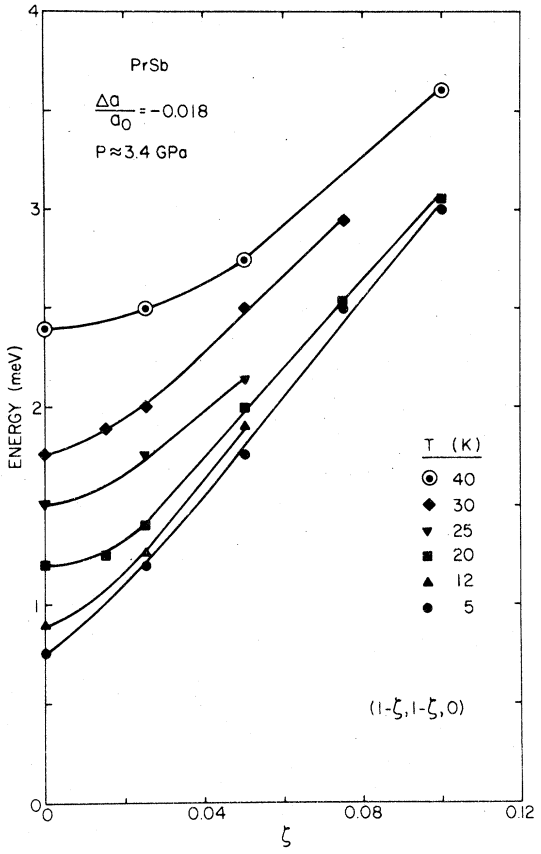

FIG. 11. Expanded view of the data near 110 in Fig. 12 showing the softening of the longitudinal exciton with decreasing temperature. $T_N = 18 \pm 1$ °K at this pressure.

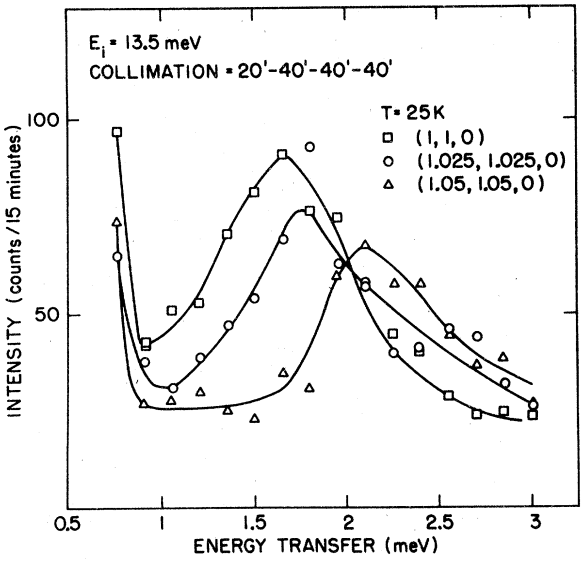

FIG. 12. Typical data for the longitudinal magnetic exciton at $T = 25$ °K and $P = 3.4$ GPa showing the smooth decrease in energy with decreasing $\vec{q}$.

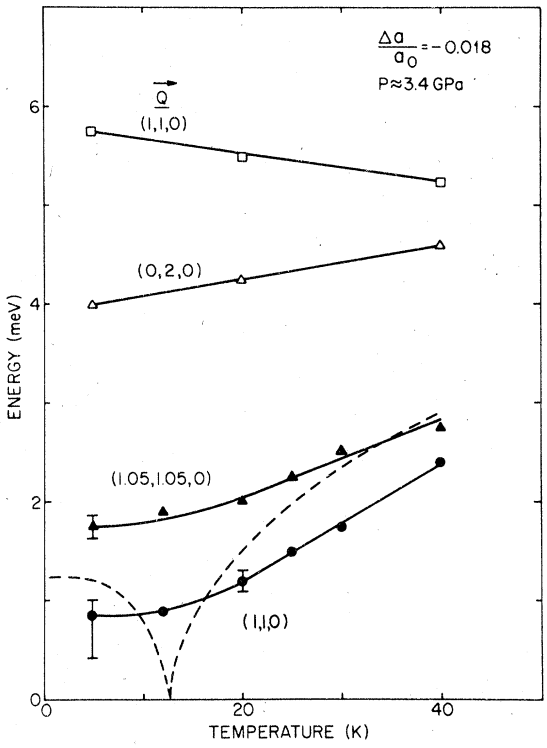

FIG. 13. Magnetic exciton energy vs temperature at $P = 3.4$ GPa where $T_N = 18 \pm 1$ °K. Solid lines are guides to the eye. The dashed curve is calculated using the RPA result for a singlet-singlet model at $\vec{Q} = (1, 1, 0)$ as described in the text.

than about 0.75 meV. Second, the mode softens continuously with decreasing temperature, rather than stopping for some $T > T_N$. Finally, it is impossible to reconcile the dispersion curve at larger q with a zero gap, without assuming an anomalous q dependence of the excitation.

V. DISCUSSION

In the limit of $T \rightarrow 0$ °K, PrSb approaches the idealized singlet-singlet model with antiferromagnetic exchange, because anisotropy in the exchange lifts the degeneracy of the Γ_4 triplet. In our data above the critical pressure at $T = 5$ °K, the longitudinal exciton at X has an energy of ≈ 10 °K whereas the transverse excitons are at ≈ 60 °K. This is in marked contrast to Pr_3Tl where it is assumed that the longitudinal and transverse excitons are degenerate, leading to a singlet-triplet system. There are extensive calculations in the literature for a singlet-triplet model with ferromagnetic exchange. These include predictions for both the static properties, such as ordering temperature and magnetic moment, and the spin dynamics near the transition. The parameters in the model

are the single-ion crystal field separation, Δ, and the isotropic exchange, $J(\vec{q})$. Both of these parameters are obtained for Pr_3Tl by fitting the dispersion relation for the Γ_1-Γ_4 exciton. Qualitative agreement between theory and experiment is obtained for the variation of T_c with composition in $Pr_{3-x}La_xTl$ or with pressure in Pr_3Tl. In the former it is assumed that Δ is constant and that $J(\vec{q})$ varies linearly with x. In the latter it is assumed that $J(\vec{q})$ is constant and that Δ varies as in a point-charge model. As these calculations are based on either molecular-field or collective excitation approximations, they are not expected to give quantitative agreement in the critical region at $T_c \rightarrow 0$.

The theoretical predictions for the spin dynamics include exact hydrodynamic models and RPA calculations using the full level schemes.[13–16] Broadly speaking, these calculations give two modes: a well-defined excitation at finite energies which evolves from the singlet-triplet exciton and a broad quasielastic mode which evolves from excitations within the triplet levels. With decreasing temperatures, the energy of the exciton decreases and saturates as the Curie temperature is approached, while the intensity of the mode at $\epsilon = 0$ peaks at T_c. These predictions are in qualitative agreement with existing neutron scattering results.

To the extent that PrSb approaches a singlet-singlet model at low temperatures, similar comparisons with the molecular-field model for T_c vs P and RPA calculations for the dynamics can be made. In the former, the ordering temperature is obtained by solving for T in

$$\frac{4\alpha^2 J(\vec{q})}{\Delta} = \frac{1 - e^{-\Delta/kT}}{1 + e^{-\Delta/kT}}$$

and in the latter the dispersion relation for the singlet-singlet exciton above T_N is

$$\omega(\vec{q})^2 = \Delta^2 \left[1 + \frac{4\alpha^2 J(\vec{q})}{\Delta} F(T) \right] ,$$

where

$$F(T) = \frac{1 - e^{-\Delta/kT}}{1 + e^{-\Delta/kT}} .$$

From Fig. 9 one concludes that the crystal-field splitting decreases linearly with decreasing lattice parameter with $(d\Delta/da)_{a=a_{crit}} = 16.6$. The slopes for the energy of the excitons at Γ_4, X_4, and X_5 are approximately equal, which implies that the pressure dependence of $J(\vec{q})$ is much smaller than that of Δ. The evolution of induced-moment magnetism can be calculated using two parameters, Δ_{crit} and the variation of Δ with lattice parameter. From the dispersion relation given above and the data in Fig. 10, Δ can be taken to be the energy of the exciton at a $\vec{Q}$ where it is independent of temperature [$\vec{Q} \approx (0.1, 0.1, 0)$ and $(0.75, 0.75, 0)$], i.e., where $J(\vec{q})$ is zero. This is very close to the energy of the exciton at Γ_4. The value of Δ for the onset of magnetism, Δ_{crit}, is taken from Figs. 4 and 5 to be $\Delta_{crit} = 53\,^{\circ}K$. Using the relation $4\alpha^2 J(110)/\Delta_{crit} \equiv 1$ at $T = 0$, both the phase boundary in the T-P plane and the temperature dependence of the longitudinal exciton at $\vec{Q} = (1, 1, 0)$ at $P = 3.4$ GPa can be calculated, and they are shown as the solid line in Fig. 4 and the dashed curve in Fig. 13, respectively. As with Pr_3Tl, the phase boundary is in qualitative agreement with the available data. However, the temperature dependence of the longitudinal exciton does not show the complete softening predicted by the singlet-singlet model. As the transverse excitons are at substantially higher energies, the model used to explain the absence of softening which involved excitations within the triplet centered at $\omega = 0$ is not applicable to PrSb. It is hoped that these results on what should be a model system will lead to further theoretical studies of crystal fields and induced-moment magnetism.

In conclusion, we have followed the lowest crystal-field levels in PrSb as a function of pressure and demonstrated the evolution of induced-moment antiferromagnetism as the longitudinal magnetic exciton softens. The qualitative features of the phase diagram in the temperature-pressure (volume) plane are compatible with the singlet-singlet model. The magnetic excitations near the critical region are not compatible with the singlet-singlet model. As these measurements are the first inelastic neutron scattering done above $P = 3.0$ GPa at low temperatures, it is hoped that the pressure can be made more hydrostatic in the future and that it might be possible to study the temperature renormalization of the excitons right at the critical pressure for induced-moment antiferromagnetism in the limit of $T \rightarrow 0\,^{\circ}K$.

ACKNOWLEDGMENTS

Research at BNL supported by Division of Basic Energy Sciences, DOE. Through the course of this work we have profitted from discussions with a number of people, in particular P. Bak, R. J. Birgeneau, E. I. Blount, R. A. Cowley, B. I. Halperin, and P. C. Hohenberg. We are indebted to L. D. Longinotti for growing the crystals of PrSb. We thank A. L. Stevens for technical assistance and W. R. Jones for help with mounting the strain gauges.

[1]B. R. Cooper, in *Magnetism in Metals and Metallic Compounds,* edited by J. T. Lppuszanski, A. Pekalski, and J. Przystawa (Plenum, New York, 1976), p.225.
[2]R. J. Birgeneau, in *Proceedings of the 18th Conference of Magnetism and Magnetic Materials, Denver, 1972,* edited by C. D. Graham, Jr. and J. J. Rhyne, AIP Conf. Proc. No. 10 (AIP, New York, 1973), p. 1664.
[3]K. C. Turberfield, L. Passell, R. J. Birgeneau, and E. Bucher, J. Appl. Phys. 42, 1746 (1971).
[4]K. R. Lea, M. J. M. Leask, and W. P. Wolf, J. Phys. Chem. Solids 23, 1381 (1962).
[5]R. J. Birgeneau, E. Bucher, J. P. Maita, L. Passell, and K. C. Turberfield, Phys. Rev. B 8, 5345 (1973).
[6]H. T. Weaver and J. E. Schirber, in *Proceedings of the 20th Conference on Magnetism and Magnetic Materials, San Francisco, 1974,* edited by C. D. Graham, Jr., G. H. Lander, and J. J. Rhyne, AIP Conf. Proc. No. 24 (AIP, New York, 1975), p. 49; Phys. Rev. B 14, 951 (1976).
[7]R. P. Guertin, J. E. Crow, L. D. Longinotti, E. Bucher, L. Kupferberg, and S. Foner, Phys. Rev. B 12, 1005 (1975).
[8]C. Vettier, D. B. McWhan, E. I. Blount, and G. Shirane, Phys. Rev. Lett. 39, 1028 (1977).
[9]B. R. Cooper and O. Vogt, Phys. Rev. B 1, 1218 (1970).
[10]K. Andres, E. Bucher, S. Darack, and J. P. Maita, Phys. Rev. B 6, 2716 (1972).
[11]R. P. Guertin, J. E. Crow, F. P. Missell, and S. Foner, Phys. Rev. B 17, 2183 (1978).
[12]R. J. Birgeneau, J. Als-Nielsen, and E. Bucher, Phys. Rev. Lett. 27, 1530 (1971); Phys. Rev. B 6, 2724 (1972).
[13]S. R. P. Smith, J. Phys. C 5, L157 (1972).
[14]M. E. Lines, J. Phys. C 7, L282 (1974).
[15]W. J. L. Buyers, in *Proceedings of the 20th Conference on Magnetism and Magnetic Materials, San Francisco, 1974,* edited by C. D. Graham, Jr., G. H. Lander, and J. J. Rhyne, AIP Conf. Proc. No. 24 (AIP, New York, 1975), p. 27.
[16]P. C. Hohenberg and J. B. Swift, J. Phys. C 7, 4009 (1974).
[17]J. Als-Nielsen, J. K. Kjems, W. J. L. Buyers, and R. J. Birgeneau, J. Phys. C 10, 2673 (1977).
[18]D. Bloch, J. Paureau, J. Voiron, and G. Parisot, Rev. Sci. Instrum. 47, 296 (1976).
[19]R. Delaplace, G. Malfait, and D. Jerome, Rev. Phys. Appliq. 11, 327 (1976).
[20]D. L. Decker, J. Appl. Phys. 42, 3239 (1971).
[21]R. A. Miller and D. E. Schuele, J. Phys. Chem. Solids 30, 589 (1969).
[22]M. E. Mullen, B. Lüthi, P. S. Wang, E. Bucher, L. D. Longinotti, and J. P. Maita, Phys. Rev. B 10, 186 (1974).
[23]D. B. McWhan, C. Vettier, L. D. Longinotti, and G. Shirane, Phys. Rev. B 18, 4540 (1978).
[24]N. Wakabayashi and A. Furrer, Phys. Rev. B 13, 4343 (1976).
[25]M. Blume, A. J. Freeman, and R. E. Watson, J. Chem. Phys. 37, 1245 (1962).
[26]G. E. Bacon, Acta Crystallogr. Sect. A 28, 357 (1972).
[27]W. Marshall and S. W. Lovesey, *Theory of Thermal Neutron Scattering* (Clarendon, Oxford, 1971).
[28]E. Umlauf, P. Holzer, J. Keller, M. Dietrich, W. Gey, and R. Meier, Z. Phys. 271, 305 (1974).
[29]H. R. Ott, in *High Pressure and Low Temperature Physics,* edited by C. W. Chu and J. A. Woollam (Plenum, New York, 1977), p. 205.